THE SUPERNOVA REMNANT RCW 103 AT RADIO WAVELENGTHS

JOHN R. DICKEL
Astronomy Department, University of Illinois, 1002 West Green Street, Urbana Illinois 61801
Electronic mail: johnd@astro.uiuc.edu

ANNE GREEN AND TAISHENG YE
School of Physics, University of Sydney, Sydney, N.S.W. 2006, Australia
Electronic mail: a.green@physics.usyd.edu au and t.ye@physics.usyd.edu.au

D. K. MILNE
Australia Telescope National Facility, CSIRO, Box 76, Epping, N.S.W. 2121, Australia
Electronic mail: dmilne@atnf.csiro.au

Received 1995 August 8; revised 1995 September 26

ABSTRACT

High-resolution radio polarimetry of the Galactic supernova remnant RCW 103 shows a nearly circular, fairly thick shell. A number of thin filaments appear throughout the shell; they match perfectly the filamentary structure seen at optical wavelengths. We have found no evidence for a point x-ray source seen in the center of the remnant by the Einstein Observatory. The observed polarization is weak and is present only at a few spots which do not correspond with the brightest regions seen in total intensity. However, at all locations where polarization is observed, the orientation of the magnetic field is nearly the same. These data indicate that RCW 103 has recently entered the point-blast stage in its evolution. © *1996 American Astronomical Society.*

1. INTRODUCTION

RCW 103 (G332.4−0.4) is a well-known Galactic supernova remnant (SNR). Images of the radio synchrotron emission show an almost complete, almost circular shell with a diameter of about 9′ (Caswell *et al.* 1980). Filaments seen in optical spectral lines are prominent toward the brighter regions of the radio shell (van den Bergh *et al.* 1973). In addition, particularly on the southern side, the remnant appears to be interacting with a molecular cloud observed in the 2.122 μm line of H_2 and other infrared lines (Burton & Spyromilio 1993; Oliva *et al.* 1990). A faint shell similar in outline to the brightest parts of the radio shell of RCW 103 was seen by Touhy & Garmire (1980) using the High-Resolution Imager (HRI) of the Einstein Observatory. They also detected an unresolved x-ray source in the center of the remnant. However, new x-ray observations with the HRI and PSPC detectors on *ROSAT* do not show this central source (Becker *et al.* 1993).

These morphological properties present conflicting evidence for classifying the evolutionary stage of this SNR. The generally circular structure suggests that the remnant is fairly young, not having had time to become distorted by the irregular surrounding medium. The shell x-ray structure is also characteristic of SNRs in the young double-shock stage of their evolution (Chevalier 1982). A forward shock leads the expansion of the piston and a reverse shock ploughing back into the ejecta is responsible for most of the heating producing the x-ray emission. On the other hand, a good correlation of the optical and near-infrared line emission with the radio filaments does not occur until later when the remnant is in the point-blast stage in the evolution of an SNR (Sedov 1959), and compressed filaments become visible in both wavelength regimes. This relation between the views of the filaments at different wavelengths was first discussed in detail by Duin & van der Laan (1975) and no known remnants violate it. The radio spectral index of −0.55 (Caswell *et al.* 1980) is also intermediate between steeper values for historical remnants and flatter ones for older remnants (Dickel 1991).

The distance to RCW 103, and thus knowledge of its linear size, is somewhat uncertain. Caswell *et al.* (1975) saw 21 cm hydrogen-line absorption out to a velocity of -44 km s^{-1} which corresponds to a distance of 3.3 kpc along that line of sight in the Galaxy. There is no further absorption out to the tangent point at 8.9 kpc at a velocity of 105 km s^{-1}. On the other hand, the visual extinction toward the SNR is 4.5 mag (Leibowitz & Danziger 1983), which corresponds to a distance of 6.6 kpc using a mean Galactic absorption. Both the mean extinction and the distribution of neutral hydrogen clouds in the Galaxy are certainly variable. We will adopt the hydrogen-line absorption value. However, this is a lower limit, and the distance could be larger if there is a lack of neutral hydrogen clouds in the clumpy interstellar medium to some greater distance along the particular line of sight to RCW 103. At the adopted distance of 3.3 kpc the diameter of 9′ corresponds to 8.6 pc, which is reasonable for a remnant near the transition between the double-shock and point-blast evolutionary stages.

Radio polarimetry with 2.4′ resolution at 3 cm wave-

 0004-6256/96/111(1)/340/6/$6.00

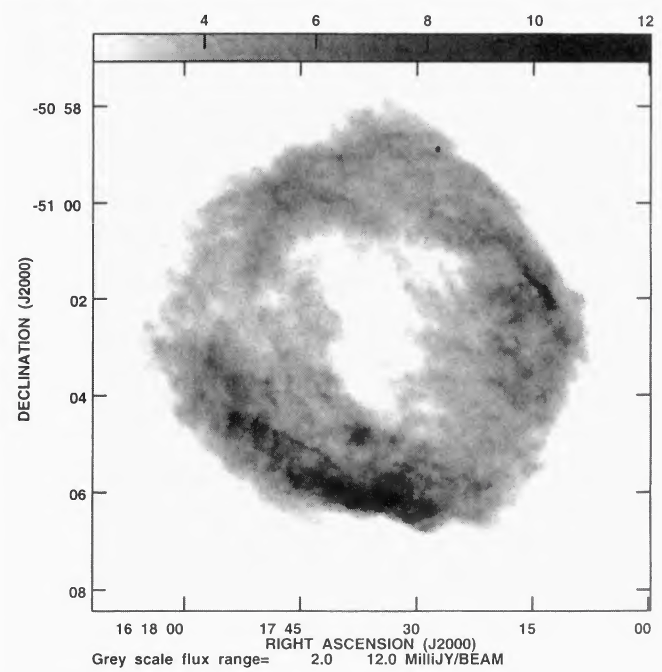

FIG. 1. Greyscale image of the supernova remnant RCW 103 at a frequency of 2372 MHz (12.65 cm wavelength). The half-power beamwidth was 4.5″.

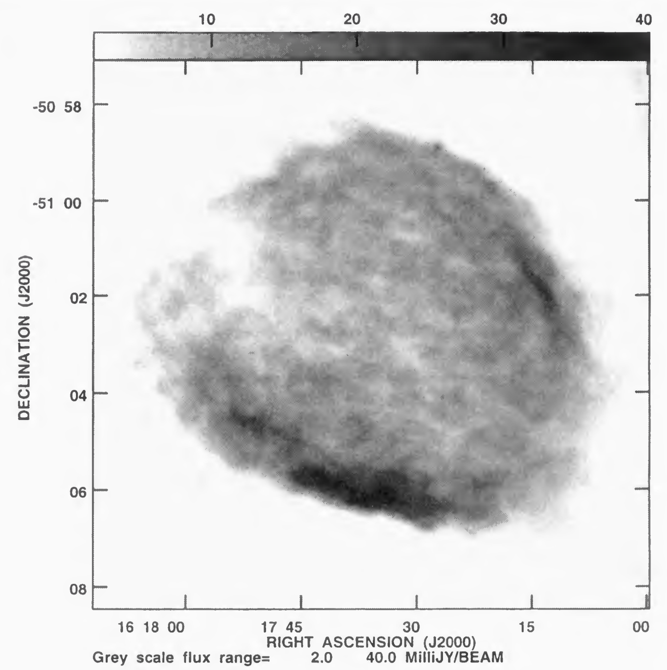

FIG. 2. Greyscale image of the supernova remnant RCW 103 at a frequency of 1362 MHz (22.03 cm wavelength). The half-power beamwidth was 8.0″.

length, using the Parkes telescope (D. K. Milne 1995 in preparation), has shown that the emission from RCW 103 is significantly polarized but the fine structure of the magnetic field, which can help elucidate the evolutionary stage, is not known. To determine this structure and also to see if the apparent correspondence of the radio and optical features is actually a detailed match of individual filaments, higher-resolution radio images have been made with the Australia Telescope Compact Array (ATCA). These data give us the first detailed radio picture of this SNR. We also derive an upper limit to any radio emission associated with the mysterious point x-ray source in the center of the remnant. The observations and data reduction are described in Sec. 2, and the results are given in Sec. 3 and discussed in Sec. 4.

2. OBSERVATIONS AND DATA REDUCTION

The observations were made in 1993 with four configurations of the ATCA (Australia Telescope 1992) at frequencies of 2372 and 1362 MHz. The spacings of the six 22 m radio telescopes extended over the range 31–6000 m. The total bandwidth of 128 MHz at each frequency was broken into 32 channels of 4 MHz each to allow narrowband interference to be removed and to eliminate bandwidth smearing of the measured visibilities. After editing, the final bandwidth used was 96 MHz at 2372 MHz and 64 MHz at 1362 MHz.

The primary calibration source was PKS 1934−638 which had flux densities of 11.57 and 14.98 Jy at 2372 and 1362 MHz, respectively (Reynolds 1994). The secondary calibrator for phase and polarization was PKS 1600−48. The position of that source was poorly known during the first observing run in 1993 May but those data were used to correct the position relative to PKS 1934−638. That data set was then appropriately offset and the correct position used in the subsequent observing sessions. The final position we determined for 1600−48 is $16^h03^m50\overset{s}{.}688$ and $-49°04'05.74''$ (J2000).

Because RCW 103 is quite extended, it filled a sizeable portion of the main beam of the individual AT antennas. Therefore we applied a primary beam correction to the final maps of the SNR. The correction was about 10% at the outer edges of the shell on the 2372 MHz map, and $2\frac{1}{2}\%$ at the edge of the remnant at 1362 MHz.

RCW 103, at $l=332.4°$ and $b=-0.4°$, lies in a complex region of the Galaxy and its emission is significantly contaminated by the presence of other nearby sources. In particular, the H II region G332.2−0.4 lies about 17′ southwest of RCW 103 and has a brightness about five times greater than RCW 103 at both frequencies, despite the fact that it lies well outside the half-power point of the primary beam at 2372 MHz, and about at the half-power point at 1362 MHz. G322.2−0.4 was included in the various maps constructed but the presence of this somewhat extended source on the steep gradient of the primary beam made CLEANing or any attempts at self-calibration very difficult, and ultimately limited the sensitivity of the observations, particularly in the polarization. Only features brighter than about 1 mJy beam^{-1} is generally considered reliable on the final maps at both frequencies.

3. RESULTS

3.1 Total-Intensity Maps

Greyscale versions of the total-intensity maps at 2372 and 1362 MHz are shown in Figs. 1 and 2, respectively. They both show a nearly complete shell of smooth emission with very filamentary structure superimposed. There is a one-to-one correspondence of the radio filaments with those seen at optical and near-infrared wavelengths, although there can be

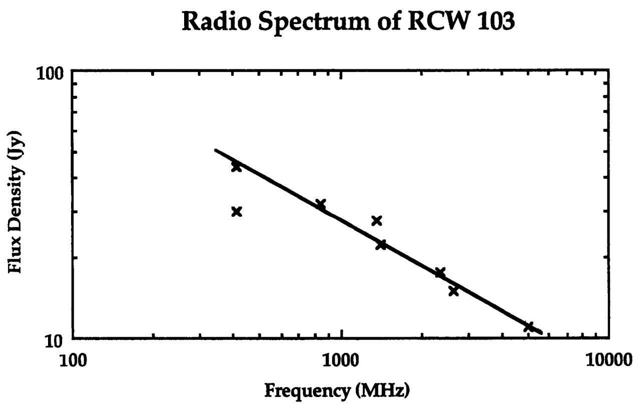

FIG. 3. Radio spectrum of RCW 103. The data are from: 408 MHz (Kesteven 1968), (Shaver & Goss 1970); 843 MHz (Whiteoak 1993); 1362 MHz (this paper); 1415 MHz (Caswell *et al.* 1980); 2372 MHz (this paper); 2650 MHz (Beard 1966); 5000 MHz (Goss & Shaver 1970).

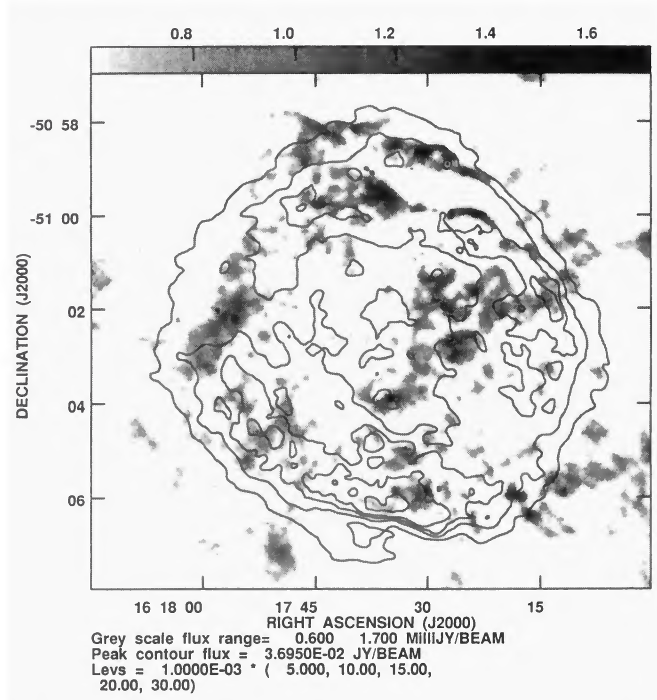

FIG. 4. Greyscale image of the polarized intensity of RCW 103 at 2372 MHz superimposed on contours of the total intensity. The half-power beamwidth was 8.0″.

some variation of the relative intensities. This structure is very similar to that of older remnants such as IC 443 (Mufson *et al.* 1986) and the Cygnus Loop (Dickel & Willis 1980). Many of the filaments, including the prominent long filament on the inner side of the shell in the southeast, are unresolved with the 4.5″ half-power beamwidth of the 2372 MHz observations. With our adopted distance of 3.3 kpc this resolution corresponds to a linear scale of 0.07 pc.

The integrated flux densities of RCW 103 at the two frequencies are difficult to determine accurately from the ATCA maps because of the large size of the source. At 2372 MHz, the shortest 31 m spacing corresponds to a ripple with an angular wavelength of 14′, and so the source appeared to sit on an extended region with an amplitude of $\sim$1.5 mJy beam^{-1}. This value was adopted as the mean baseline level and subtracted from the observed brightness to give an integrated flux density of 17.6 Jy. This value is only slightly higher than that predicted from the spectrum compiled in Fig. 3. The fit shown has a mean spectral index of -0.56. In determining that line we chose to consider that Kesteven's (1968) value of 30 Jy at 408 MHz was low, and adopted only the flux density of 44 Jy at the frequency measured by Shaver & Goss (1970) using the same instrument.

At 1362 MHz, the 31 m spacing was unusable because of continual interference. therefore, the shortest available baseline was 61 m, which gave a ripple of 10′ wavelength. This was too close to the size of RCW 103 to remove its effects reliably and so the integrated flux density found of 27.5 Jy can be uncertain by up to 30%, which is greater than its deviation from the mean spectrum. Eliminating this 1362 MHz ATCA point from the fit makes virtually no difference. The lack of the short spacing at 1362 MHz also made it impossible to construct a spectral index map of RCW 103. However, the spectral index of all the bright features on the southern, western, and northern parts of the shell do not deviate significantly from the mean value of -0.56.

Neither image shows the central Einstein x-ray point source at $16^{h}17^{m}48^{s}.3$ and $-51°02'26''$ (J2000) (Tuohy *et al.* 1983). The 3σ upper limits to any radio emission from this position are 0.1 mJy at 2372 MHz and 0.6 mJy at 1362 MHz. These limits are smaller than the uncertainties for the general structure described above because the background does not vary significantly over the small area in the center of the remnant which was searched for a point source. The values given are three times the rms noise over a 1′ square box centered at the given position. Attempts to fit Gaussians within this region gave values $<1\sigma$. We note that the source is also not present on the more recent *ROSAT* images by Becker *et al.* (1993) although they conclude that it still could be a cooling neutron star with a lower temperature than suggested by Tuohy *et al.* (1983).

3.2 Polarized Emission

For the polarization analysis, all the data must be at the same resolution. We therefore convolved the original Q and U images to circular Gaussians with a half-power width of 8″ (the beamwidth at the lowest frequency used). Few of the polarized intensities were strong enough to be significantly above the noise level but a small amount of CLEANing was applied to each map (about 1000 iterations with a loop gain of 0.01) to remove sidelobes of the brighter points. The data were then combined to give position angle and polarized intensity maps. Statistical corrections for the bias created by the combination of positive and negative vectors in the presence of noise was applied using the AIPS routine POLCO. The rms noise levels measured on the final cleaned, convolved Q and U maps were 0.3 and 0.1 mJy at 2372 and 1362 MHz, respectively. The position-angle plots which were used to determine the Faraday rotation were truncated if the corrected polarized intensities were less than 0.9 mJy beam^{-1} at 2372 MHz and 0.4 mJy beam^{-1} at 1362 MHz.

The polarized intensities recorded at both wavelengths are very low but the detected signals are definitely stronger to-

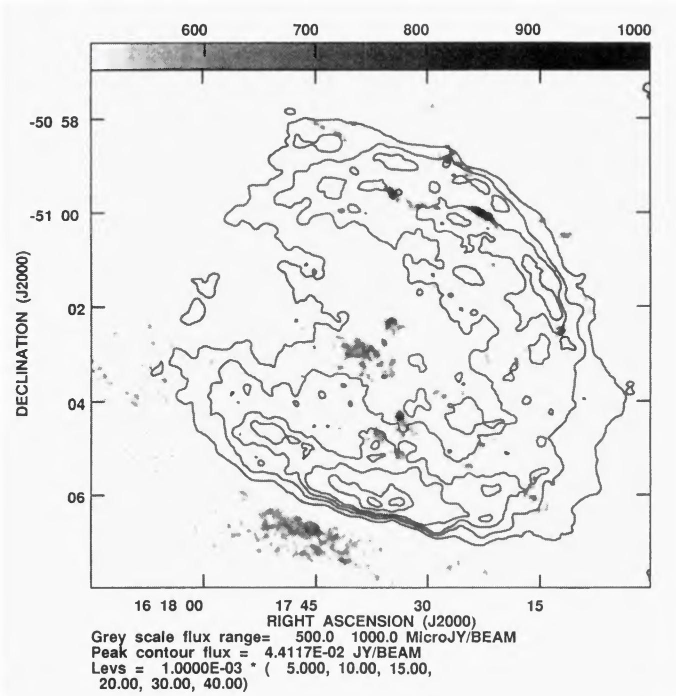

FIG. 5. Greyscale image of the polarized intensity of RCW 103 at 1362 MHz superimposed on contours of the total intensity. The half-power beamwidth was 8.0″.

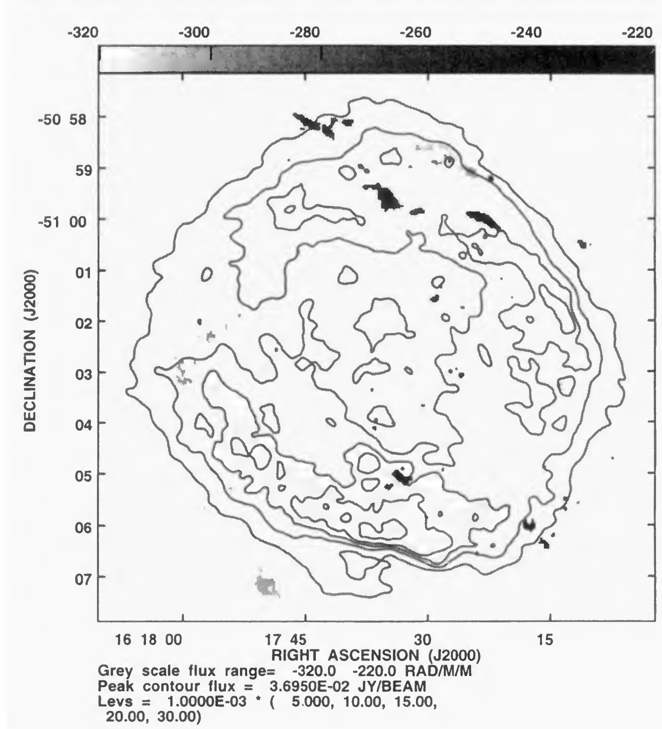

FIG. 6. Faraday rotation toward RCW 103.

ward RCW 103 than off the source. At 2372 MHz all points brighter than 1.3 mJy beam^{-1} (four times the cutoff determined by the polarization correction program) lie within the SNR, and the average polarized intensity on the source is 60 μJy beam^{-1} brighter than the average in the region of the map off the source. At 1362 MHz where the polarized signal is weaker, the upper limit to the polarized brightness off source is 0.7 mJy beam^{-1} (three times the POLCO cutoff) and the average value of the polarized intensity on source is 30 μJy beam^{-1} greater than off source. At least some of the polarized emission must be from the SNR and not the background.

Greyscale renditions are shown superimposed on total-intensity contours in Figs. 4 and 5. These images illustrate that the emission is in small clumps and have little or no correlation with total-intensity features. The fractional polarization varies over the source with no obvious pattern. At 2372 MHz it varies from less than 1% on the brightest filaments to 31% at $16^{\rm h}17^{\rm m}40^{\rm s}$ and $-51°04'$ (J2000) near the center of the remnant where the polarized intensity is strong but the total intensity is weak. The range in polarized fraction is less at 1362 MHz. The mean depolarization ratio between the two frequencies is 1.9, indicating only a small amount of internal depolarization in this remnant. Because the single-dish polarization measured with a resolution of 2.4′ at 3 cm (D. K. Milne 1995 in preparation) is high, the results indicate that most of the polarized intensity is reasonably uniform over large sections of the remnant. It is apparently more uniform than the total intensity, and the interferometer sees only the significant small-scale deviations from this generally smooth polarized contribution. An attempt at natural weighting of the UV visibilities before Fourier transforming to make the polarized maps was unsuccessful because of the very strong contributions from the confusing sources near the half-power points of the primary beams. This very patchy polarization structure observed at high resolution is reminiscent of that seen for the adolescent SNR IC 443 (Wood *et al.* 1991) but unlike the nearly uniform distribution of fine-scale cells seen in young remnants, such as Tycho's SNR (Dickel *et al.* 1991).

To determine the orientation of the magnetic field in the remnant we need to determine the Faraday rotation from the measured position angles and extrapolate back the position angles at zero wavelength. The two observed central frequencies are far enough apart that there can be $n\pi$ rotations in position angle between them. Therefore, to remove this ambiguity in the measured position-angle differences, we have broken the original data into parts and produced polarization Q and U maps at the four frequencies of 2410, 2338, 1385, and 1341 MHz. These data had limited bandwidths of 24 MHz at 2410 and 2338 MHz, and 20 MHz at 1385 and 1341 MHz. Hence, the signal-to-noise ratio was low. The four-frequency results were sufficient, however, to show the position-angle differences between the central frequencies of the two full-bandwidth results. The differences in position angle between the two central frequencies ($\mathrm{P.A.}_{2372\ \mathrm{MHz}} - \mathrm{P.A.}_{1362\ \mathrm{MHz}}$) were equal to the measured values $+\pi$ radians. The final analysis used the two-frequency measurements with the additional π radians inserted.

The final Faraday rotation map (Fig. 6) is, of course, sparse but shows a consistent mean rotation near -250 rad m^{-2} at all locations in the remnant. It is probably a small foreground rotation. One intriguing region at $16^{\rm h}17^{\rm m}23^{\rm s}$ and $-51°00'02''$ (J2000) shows a slight apparent gradient from east to west across the filament of about 25 rad m^{-2} in about 40″ which corresponds to about 0.65 pc. This small rotation gives a product N_e B dl of only 3×10^{-5} cm^{-3} Gauss pc, so a trivial change in any one parameter can cause the observed

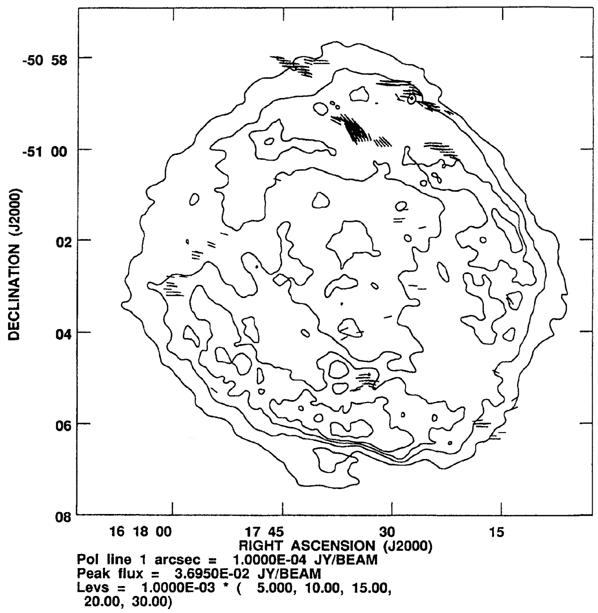

FIG. 7. Magnetic-field vectors in the supernova remnant RCW 103. The orientation indicates the direction of the magnetic field and the length represents the polarized intensity at 2362 MHz. The contours are the total intensity at 2362 MHz. The resolution was 8.0″.

variation and we cannot correlate it with any particular change in physical parameters within that feature.

The map of the magnetic field vectors is shown in Fig. 7. The orientation is that of the magnetic field direction and the vector length represents the polarized intensity at 2362 MHz. The field appears to have a general east-west orientation across the entire remnant with the most notable deviation at the position of the brightest polarized feature at $16^h17^m35\overset{s}{.}5$ and $-51°59'34''$ (J2000). The mean Faraday rotation at that location is -250 rad m^{-2}, near the average value of the whole remnant, and there is no significant feature in the total-intensity image. D. K. Milne's higher frequency but lower-resolution results (1995 in preparation) confirm the general field orientation and Faraday rotation given here.

There is also an indication of a bulge on the outer edge of the unresolved source on the northern side of the shell at $16^h17^m27\overset{s}{.}4$ and $-51°58'53\overset{''}{.}6$ (J2000). It may be a clump in the remnant which is pushing into the overall field as a slower version of the expanding clumps in Cas A seen by Braun *et al.* (1987) or the x-ray and radio bullets seen around the edge of the Vela SNR (Aschenbach *et al.* 1995; Strom *et al.* 1995). The spectral index of this point source is about -0.6 which does not differ from the that of the rest of the remnant.

4. DISCUSSION

4.1 Structure

Although RCW 103 is encountering a cloud of enhanced molecular emission on the south (Burton & Spyromilio 1993), its outline is nearly circular, implying that the interaction must be quite recent and that the remnant's previous expansion has been relatively unimpeded. The brightening of the rim in the northern and southern sides hints of an incipient barrel shape for this SNR with a greater opening toward the eastern side. If this is so, the more or less east-west alignment of the magnetic field would represent the orientation of the magnetic field in the ambient interstellar medium. This frozen-in field would help to limit the expansion north-south and probably in the direction along the line of sight toward and/or away from the observer. It is the compression of this field which produces the increased radio emission from the SNR. The fact that the previously seen, unresolved x-ray source lies so nearly in the center of the remnant argues that, if it is related to the progenitor, it cannot have moved far and that the structure of the remnant is controlled by its only recently encountering the walls of a cavity.

The overall shell of RCW 103 is quite thick, as one might expect for a reasonably young remnant in which the reverse shock had only recently passed through the entire shell and reached the center. However, fine filamentary structure and direct match of the radio and optical filaments clearly indicate that the remnant has reached the point-blast (Sedov 1959) stage of its evolution. This conclusion is supported by the polarization structure. As discussed above, the general field direction is approximately east-west in orientation with only very few deviations. By contrast all young (double-shock) shell SNRs have a radial orientation of their magnetic field patterns (e.g., Dickel *et al.* 1988; Dickel *et al.* 1991; Reynolds & Gilmore 1993) and most old SNRs have very irregular and confused fields (Milne 1987) with a few tending toward a tangential orientation with respect to the shell (Milne & Haynes 1994). We suggest that this magnetic-field pattern also indicates that RCW 103 has just made the transition from the double shock into the point-blast evolutionary phase. The field has lost it radial character, caused by the Rayleigh–Taylor instabilities stretching at the shock interfaces, but has not yet had time to distort significantly the overall surrounding field on a smaller scale.

The mean polarization of RCW 103 shown here is very weak and, in particular, the brightest features in the total intensity show no detectable polarized signal. The total intensity depends on the magnetic-field strength and relativistic electron density while the polarized intensity is the product of two factors, the degree of linear polarization and the total intensity. The degree of linear polarization is highest when the relativistic electrons are radiating synchrotron emission along a uniform magnetic field, and vanishes when the field is completely tangled. Thus the degree of polarization depends on the organization of the field, but the total intensity depends on the magnetic-field strength (Wood *et al.* 1991). Because the magnetic field and particles are expected to track each other, the lack of correlation between the total and polarized intensities suggests that the increased polarization arises in reasonably uniform regions where the magnetic-field organization is high but the field strength is low. These are probably residual areas in the remnant where clumping and shocks have not tangled and amplified the magnetic fields to produce the strongest synchrotron radiation. Other faint areas could have moderate polarization but be too weak to detect. Presumably in the future, interactions with more clumps may further distort the general field pattern and amplify intensities.

4.2 Concluding Remarks

The data indicate that RCW 103 has only very recently made the transition from the young double-shock stage of its evolution (Chevalier 1982), which is controlled primarily by the ejected material, to the point-blast stage (Sedov 1959) mainly dependent on the swept-up surrounding material. This transition must occur very quickly as there is no hint of residual radial structure in the magnetic field of the remnant. Compression of the filaments to produce the strong radio and optical emission has also proceeded very rapidly. Such a phenomenon could occur if the remnant has indeed only recently encountered the walls of a cavity.

To understand the evolution of the remnant we need to measure the expansion rate. And to predict this we need to know the type of star that exploded (see Chevalier 1982) as well as the total age and the length of time since it entered the Sedov phase. The apparent presence of the peculiar point x-ray source at the center of the remnant and the possibility that the unresolved source on the northern rim at $16^h17^m27\overset{s}{.}4$ and $-51°58'53\overset{''}{.}6$ (J2000) might be an outward-moving clump distorting the magnetic field within the SNR suggest that RCW 103 was the result of an explosion of a massive star. This would imply an expansion in radius proportional to $t^{0.9}$ (Chevalier 1982). If the remnant has been expanding at this rate from a radius of 0.01 pc and velocity of 10 000 km s^{-1} one year after the explosion, then its age is about 1000 years and the current speed is about 5000 km s^{-1} or 0.005 pc yr^{-1}. This rate is about 0.2″ yr^{-1} or 1/2 beamwidth in 10 years. A repeat measurement should be made in about the year 2003 to look for the expansion.

We thank Y.-H. Chu, M. Anderson, W. Becker, and S. Casertano for information and help in preparing the paper. JRD was partly supported by the US National Science Foundation Grant No. INT 91-14551 and NASA Grants Nos. HST-AR-5295.01-93A and NAG 5-2245.

REFERENCES

Australia Telescope 1992, J. Elec. Electron. Eng., Australia, 12, No. 2, (special issue on the Australia Telescope)
Aschenbach, B., Eggers, R., & Truemper, J. 1995, Nature, 373, 587
Beard, M. 1966, Australian J. Phys., 19, 141
Becker, W., Truemper, J., Hasinger, J., & Aschenbach, B. 1993, in Isolated Pulsars, edited by K. A. Van Riper, R. I. Epstein, and C. Ho (Cambridge University Press, Cambridge), p. 116
Bergh, S. van Den, Marscher, A., & Terzian, Y. 1973, ApJS, 26, 19
Braun, R., Gull, S. F., & Perley, R. A. 1987, Nature, 327, 395
Burton, M. G., & Spyromilio, J. 1993, Proc. Astron. Soc. Australia, 10, 327
Caswell, J. L., Haynes, R. F., Milne, D. K., & Wellington, K. 1980, MNRAS, 190, 881
Caswell, J. L., Roger, R. S., Murray, J. D., Cole, D. J., & Cook, D. J. 1975, A&A, 45, 239
Chevalier, R. A. 1982, ApJ, 258, 790
Dickel, J. R. 1991, in Supernovae, edited by S. Woosley (Springer, New York), p. 675
Dickel, J. R., van Breugel, W. J. M., & Strom, R. G. 1991, AJ, 101, 2151
Dickel, J. R., Sault, R., Arendt, R. G., Matsui, Y., & Korista, K. T. 1988, ApJ, 330, 254
Dickel, J. R., & Willis, A. G. 1980, A&A, 85, 55
Duin, R. M., & van der Laan H., 1975, A&A, 40, 111
Goss, W. M., & Shaver, P. A. 1970, Australian J. Phys., Astrophys. Suppl., No. 14, 1
Kesteven, M. J. 1968, Australian J. Phys., 21, 369
Leibowitz, E. M., & Danziger, I. J. 1983, MNRAS, 204, 273
Milne, D. K. 1987, Australian J. Phys., 40, 771
Milne, D. K., & Haynes, R. F. 1994, MNRAS, 270, 106
Mufson, S. L., McCollough, M. L., Dickel, J. R., Petre, R., White, S. L., & Chevalier, R. A. 1986, AJ, 92, 1349
Oliva, E., Moorwood, A. F. M., & Danziger, I. J. 1990, A&A, 240, 453
Reynolds, J. E. 1994, AT Doc. Ser. No. AT/39.3/040, Australia Telescope National Facility
Reynolds, S. P., & Gilmore, D. 1993, AJ, 106, 272
Sedov, L. 1959, Similarity and Dimensional Methods in Mechanics (Academic, New York), p. 210
Shaver, P. A., & Goss, W. M. 1970, Australian J. Phys., Astrophys. Suppl., No. 14, 77
Strom, R. G., Johnston, H. M., Verbunt, F., & Aschenbach, B. 1995, Nature, 373, 590
Tuohy, I. R., & Garmire, G. P. 1980, ApJ, 239, L107
Tuohy, I. R., Garmire, G. P., Manchester, R. N., & Dopita, M. A. 1983, ApJ, 268, 778
Whiteoak, J. B. Z. 1993, Ph.D. thesis, University of Sydney
Wood, C. A., Mufson, S. L., & Dickel, J. R. 1991, AJ, 102, 224